

SIMULATION OF FeCO₃/ FeS SCALE FORMATION USING THERMODYNAMIC AND ELECTROCHEMICAL MODELS

Andrzej Anderko
OLI Systems Inc.
108 American Road
Morris Plains, NJ 07950

ABSTRACT

A comprehensive model has been developed for simulating the effect of FeCO₃ and FeS scale formation on general corrosion of iron and carbon steel. The model combines thermodynamic speciation with electrochemical computations based on the mixed-potential theory. The effect of scaling is modeled by considering surface reactions between the metal and active solution species, which lead to the formation and dissolution of scales. The electrochemical computations take into account various partial anodic and cathodic processes on the metal surface, such as oxidation of iron and reduction of protons, water molecules, carbonic acid and hydrogen sulfide. The rates of the electrochemical processes are related to the presence of surface scales. The model has been verified by comparing calculated corrosion rates with experimental data over substantial ranges of environmental conditions. Good agreement with the data has been obtained. In particular, the model quantitatively reproduces the effect of variations in temperature, pH and partial pressures of CO₂ and H₂S on the formation of scales and corrosion rates.

INTRODUCTION

Formation of iron carbonate and iron sulfide scales has a profound influence on the corrosion behavior of carbon steels. Therefore, numerous experimental studies have been performed to elucidate the conditions that are conducive to the formation of FeCO₃ and FeS and to explain their effect on corrosion.¹⁻¹⁹ The formation of FeCO₃ and FeS scales depends on multiple factors including temperature, partial pressures of CO₂ and H₂S, pH, composition of the aqueous stream and flow characteristics. Therefore, it is desirable to develop a model that could rationalize the effect of these factors and to predict the effect of scale formation on corrosion rates.

In a previous study,²⁰ the stability of various solid phases that result from CO₂/H₂S corrosion was investigated. For this purpose, a comprehensive thermodynamic model was used in conjunction with a facility to generate stability diagrams,²¹ which help to visualize the conditions at which various solids are stable or metastable. In particular, it was shown, in a qualitative way, that the predicted formation of scales may explain the reduction in corrosion rates under some conditions.

The objective of this study is to develop a model that predicts the effect of scale formation on corrosion rates in a quantitative way. For this purpose, it is necessary to go beyond thermodynamic analysis and introduce an electrochemical model that simulates the kinetics of various phenomena at the metal/solution interface. In particular, this model should introduce a mathematical formalism that makes it possible to simulate the formation of scales on the metal surface and not

only in the bulk solution. Also, the model should incorporate the kinetics of various partial anodic and cathodic processes on the metal surface and should predict how such processes are influenced by the formation of scales.

THERMODYNAMIC CALCULATIONS

The starting point for the analysis of scaling and corrosion is the computation of speciation in the investigated system. For this purpose, a realistic model of electrolyte systems is used. This model combines information about standard-state properties of all species that may exist in the system with a formulation for the excess Gibbs energy, which accounts for solution nonideality. The model has been described in detail by Zemaitis et al.²² and Rafal et al.²³ In a previous study, this model was shown to predict the conditions under which various FeS and FeCO₃ scales are stable. Here, the essential elements of the model are summarized in Appendix A.

The speciation calculations define which species are present in the liquid phase and which solids may precipitate from the bulk solution. Further, the thermodynamic model predicts the concentrations and activities of both ionic and neutral species. The activities of individual species are further used in the electrochemical model.

KINETIC MODEL OF SCALE FORMATION

The precipitation of sparingly soluble species such as FeCO₃ or FeS from the bulk solution is governed by the activities of ions in the solution. For example, the reaction of precipitation of FeCO₃ can be written as



and is characterized by an equilibrium constant defined by

$$K_{\text{FeCO}_3}(T) = a_{\text{Fe}^{2+}} a_{\text{CO}_3^{2-}} \quad (2)$$

where the activities of the Fe²⁺ and CO₃²⁻ ions are consistent with the thermodynamic aqueous speciation model.

However, the mechanism of the formation of an adherent surface film is somewhat different from the mechanism of the precipitation of the same solid from the bulk solution. This is due to the fact that the thermodynamic properties of adherent surface scales are somewhat different from the properties of bulk crystals. Therefore, the reaction of formation of an FeCO₃ surface scale can be written as



where the symbol “≡” denotes the metal substrate and, therefore, ≡FeCO₃ is a species deposited on the solid surface. In particular, the formation of ≡FeCO₃ may result from the dissolution of the iron substrate, i.e.,



Reaction (4) is an electrochemical process, which can be more conveniently described in terms of electrochemical kinetics rather than equilibrium thermodynamics. In this section, we develop a mathematical formalism for reaction (4) and similar processes.

Metal dissolution in the presence of solid scales is an inherently complex process. In general, this process results from the superposition of a number of phenomena, i.e.,

- (1) Formation of scales on the metal surface;
- (2) Anodic dissolution processes that occur on the free surface of the metal and lead to the generation of metal ions;
- (3) Dissolution of the solid scales;
- (4) Cathodic processes on the free metal surface;
- (5) Cathodic processes on the scale surface, which are expected to be considerably slower than those on the free surface;

- (6) Local change in concentration of active ions close to the metal surface, which is influenced by adsorption and mass transfer and
 (7) Transport of ions through the scale, which depends on the permeability of the solid precipitate.

In principle, it is possible to develop a truly comprehensive model that takes into account all of these phenomena. However, such a model would contain a very large number of parameters that could not be predicted from first principles or unequivocally determined on the basis of the limited amount of electrochemical and exposure data that are available in the literature. Therefore, a simplified approach is necessary. For this purpose, we introduce an average fraction of the metal surface that is covered by a scale. Further, we assume that the anodic and cathodic processes that are associated with metal dissolution occur only on the fraction of the surface that is not covered by the scale. This is equivalent to assuming that the scale coverage fraction represents only a protective scale and does not include nonprotective scales. With this simplifying assumption, it is not necessary to treat explicitly the permeability of the solid precipitate. Further, the model recognizes the local concentrations of active species in the vicinity of the surface. The local concentration is introduced by considering adsorption equilibria on the surface, which precede the formation of the deposit. For simplicity, the adsorption equilibria are assumed to be the same on the scale-covered and uncovered fractions of the surface.

To derive a mathematical model that represents the effects of scale formation on corrosion rates, we consider n separate species that may be formed on the surface of the corroding metal. The fraction of the surface occupied by i -th species is denoted by θ_i . The change of the coverage fraction θ_i with time, at a constant potential and for fixed activities of solution species, can be expressed as:

$$\left(\frac{\partial \theta_i}{\partial t} \right)_{E,a} = j_i \left(1 - \sum_{k=1}^n \theta_k \right) - l_i \theta_i \quad i = 1, \dots, n \quad (5)$$

where j_i is the rate constant for the formation of the i -th species on the free surface of the metal and l_i is the rate constant for the dissolution of this species. The rate of dissolution is proportional to the fraction of the surface covered by the i -th species. Eq. (5) is a system of n ordinary differential equations. This system may be solved for the coverage fractions θ_i . In the limit of stationary state (i.e., for $t \rightarrow \infty$), the solution is

$$\theta_i = \frac{j_i}{l_i \left(1 + \sum_{k=1}^n \frac{j_k}{l_k} \right)} \quad (6)$$

In general, the rates of scale formation depend on the activities of species that promote the precipitation of the scales. Thus, j_k can be rewritten as

$$j_k = j_k^* \sigma_X^a \sigma_Y^b \dots \quad (7)$$

where σ_X , σ_Y , etc., are surface concentrations of appropriate active solution species and a , b , etc., are reaction orders. In general, there can be any number of the species X , Y , etc. The surface concentrations of the active ions result from adsorption processes on both the covered and free surfaces. Assuming the Langmuir adsorption behavior, σ_X can be expressed as

$$\sigma_X = \frac{K_X a_X}{1 + \sum_r K_r a_r} \quad (8)$$

where K_x is a constant that characterizes the adsorption of the active species that is responsible for scale formation.

The presence of scales modifies the current densities of the partial anodic and cathodic processes that are responsible for corrosion. Such processes include the anodic dissolution of iron and reduction of protons or water molecules or carbonic acid. They will be discussed in detail in the next section. To relate the kinetics of partial

electrochemical processes to scale formation, it can be assumed that the total surface area that is available for electrochemical reactions is reduced by the presence of scales, i.e.,

$$i' = i \left(1 - \sum_{k=1}^n \theta_k \right) \quad (9)$$

where i denotes any of the partial current densities that are influenced by scales and i' is its value modified by the presence scales. Eq. (9) is a simplification because it implicitly assumes that the electrochemical processes do not proceed on the fraction of the surface that is covered by the solid scales. In general, various processes may occur on the scale surfaces (e.g., the reduction of protons or water), although their rates are significantly different from the rates on metal surfaces. Thus, eq. (9) should be regarded as a formula that represents the averaged effect of surface scales and does not necessarily reflect the microscopic coverage of the surface. Substitution of eq. (6) into eq. (9) yields

$$i' = \frac{i}{1 + \sum_{k=1}^n \frac{j_k}{l_k}} \quad (10)$$

Substitution of eqs. (7) and (8) into eq. (10) yields

$$i' = \frac{i}{1 + \sum_{k=1}^n \frac{j_k^* \sigma_X^a \sigma_Y^b \dots}{l_k}} = \frac{i}{1 + \sum_{k=1}^n q_k \sigma_X^a \sigma_Y^b \dots} \quad (11)$$

where the symbol q_k is introduced for simplicity.

Thus, in addition to the bulk activity of species, the effect of scale formation is determined by two parameters, i.e., q_k and K_r . The parameter q_k is the ratio of the rate constants for the formation and dissolution of the scale whereas K_r characterizes the adsorption of the aqueous species that are responsible for scale formation. Since q_k is a ratio of two rate constants, it can be expected to be temperature-dependent. The temperature dependence of q_k can be expressed using an Arrhenius-type expression, i.e.,

$$q_x(T) = q_x(T_{ref}) \exp \left[- \frac{\Delta q_x}{R} \left(\frac{1}{T} - \frac{1}{T_{ref}} \right) \right] \quad (12)$$

The adsorption parameter K_X can be assumed to be independent of temperature. Thus, the parameters that are needed for the computation of the effect of a surface scale are $q_x(T_{ref})$, Δq_x and K_X .

In the case of a FeCO_3 scale, the HCO_3^- ion can be assumed to be the active species that participates in the scale formation because it is much more abundant than CO_3^{2-} in the pH region of FeCO_3 precipitation. Thus, eq. (4) can be rewritten in a thermodynamically equivalent form, i.e.,



Thus, $\sigma_{\text{HCO}_3^-}$ is substituted for the term $\sigma_X^a \sigma_Y^b$ in eq. (11). Since $\sigma_{\text{HCO}_3^-}$ depends on the activity of HCO_3^- ions, it is a strong function of solution chemistry. Similarly, the HS^- ions are considered to be the primary surface species that participate in the formation of FeS scales, i.e.,



If both FeCO_3 and FeS can be formed, the sum in the denominator of eq. (11) can be expressed as

$$\sum_{k=1}^n q_k \sigma_X^a \sigma_Y^b \dots = q_{FeCO_3} \sigma_{HCO_3^-} + q_{FeS} \sigma_{HS^-} \quad (15)$$

where the quantities $\sigma_{HCO_3^-}$ and σ_{HS^-} are calculated from eq. (8). Eq. (15) is an approximation because it does not recognize the existence of various crystalline forms of FeS. However, its validity will be verified later using experimental data.

PARTIAL ELECTROCHEMICAL REACTIONS

To apply the formalism described above to simulate the effect of scales on corrosion rates, it is necessary to define expressions for the current densities for partial anodic and cathodic processes that are significant in CO₂/H₂S corrosion. These expressions were introduced in a previous study²⁴ and are summarized here.

Cathodic Reactions

In CO₂/H₂S corrosion, cathodic processes may be due to the reduction of several proton-bearing species, including H⁺, H₂O, H₂CO₃, H₂S and HS⁻. In acidic solutions, the reduction of H⁺ is the dominant cathodic reaction:



It is generally accepted that the H⁺ reduction reaction may proceed under activation or mass transfer control.²⁵ According to basic electrochemical kinetics²⁵, the current density for H⁺ reduction can be written as

$$\frac{1}{i_H} = \frac{1}{i_{H,a}} + \frac{1}{i_{H,lim}} \quad (17)$$

where $i_{H,a}$ and $i_{H,lim}$ are the activation and limiting current densities, respectively. The activation current density for proton reduction is

$$i_{H,a} = i_H^0 \exp \left[\frac{-\alpha_H F (E - E_H^0)}{RT} \right] \quad (18)$$

where $\alpha_H = 0.5$ ²⁶ and E_H^0 is calculated from the Nernst equation in which the necessary quantities are obtained from the thermodynamic model. The exchange current density is given by

$$i_H^0 = i_H^* a_H^{0.5} a_{H_2O}^{1.4} \quad (19)$$

In eq. (19), the reaction order with respect to the activity of H⁺ has been obtained from the work of Bockris et al.²⁶ and the order with respect to H₂O has been determined by analyzing experimental data for concentrated solutions.

The limiting current density in eq. (17) results from diffusion-limited transport of protons to the metal surface and can be calculated as

$$i_{H,lim} = k_m F a_H \quad (20)$$

where k_m is the mass transfer coefficient, which depends on the flow regime and transport properties of the solution. The methods for computing k_m have been discussed in the previous paper.²⁴

In addition to the reduction of H⁺ ions, the direct reduction of water is also considered, i.e.,



Under ordinary conditions, the reaction of water reduction does not exhibit mass transfer limitations and the current density can be expressed as:

$$i_{H_2O} = i_{H_2O}^0 \exp\left[\frac{-\alpha_{H_2O} F(E - E_H^0)}{RT}\right] \quad (22)$$

As with proton reduction, $\alpha_{H_2O} = 0.5$ and the reversible potential in eq. (20) is the same as in eq. (18). Also, the reaction order with respect to water activity is the same as that for proton reduction. Thus, the exchange current density is given by

$$i_{H_2O}^0 = i_{H_2O}^* a_H^{-0.5} a_{H_2O}^{1.4} \quad (23)$$

In the presence of CO_2 , reduction of carbonic acid (H_2CO_3) provides a significant contribution to the cathodic process. Carbonic acid is formed as a result of hydration of dissolved CO_2 and is, subsequently, reduced on the surface, i.e.,^{27,28}



The H_2CO_3 reduction is under activation or chemical reaction control, i.e.,

$$\frac{1}{i_{H_2CO_3}} = \frac{1}{i_{H_2CO_3,a}} + \frac{1}{i_{H_2CO_3,lim}} \quad (25)$$

The activation current is given by

$$i_{H_2CO_3} = i_{H_2CO_3}^0 \exp\left[\frac{-\alpha_{H_2CO_3} F(E - E_H^0)}{RT}\right] \quad (26)$$

where the transfer coefficient can be assumed to be equal to that for H_2O reduction. Also, the reversible potential is equal to that for H^+ or H_2O reduction. The exchange current density for H_2CO_3 reduction can be expressed as:²⁸

$$i_{H_2CO_3}^0 = i_{H_2CO_3}^* a_{H_2CO_3} a_H^{-0.5} \quad (27)$$

The limiting current density can be calculated from an equation for processes with a rate-determining reaction in the solution.²⁵ Here, the rate-determining reaction is the hydration of CO_2 and the limiting current density is

$$i_{H_2CO_3,lim} = Fa_{H_2CO_3} (D_{H_2CO_3} K_{H_2CO_3} k_{H_2CO_3}^f)^{1/2} \quad (28)$$

where $D_{H_2CO_3}$, $K_{H_2CO_3}$ and $k_{H_2CO_3}^f$ are the diffusion coefficient of H_2CO_3 , equilibrium constant for the hydration of CO_2 and forward reaction for the hydration reaction, respectively. $D_{H_2CO_3}$ is calculated from the model of Anderko and Lencka²⁹, $K_{H_2CO_3}$ is obtained from the thermodynamic model (Appendix A) and $k_{H_2CO_3}^f$ is calculated from the temperature-dependent expression developed by Nescic et al.²⁸

When sufficient concentration of hydrogen sulfide is available in the solution, H_2S contributes to the cathodic hydrogen discharge by the overall reaction



Morris et al.¹⁵ found that a limiting current density in an acidic solution gradually disappears as the concentration of H_2S is increased. At the same time, the Tafel slope remains practically unchanged. This provides a strong indication that reaction

(29) proceeds entirely under activation control and is not limited by the diffusion of H₂S to the surface. Therefore, an expression for the partial current density for H₂S reduction has been proposed,²⁴ i.e.,

$$i_{H_2S} = i_{H_2S}^0 \exp\left[\frac{-\alpha_H F(E - E_H^0)}{RT}\right] \quad (30)$$

where the transfer coefficient is identical to that for proton reduction and the exchange current density is proportional to the activity of dissolved H₂S, i.e.,

$$i_{H_2S}^0 = i_{H_2S}^* a_{H_2S} a_{H_2O}^{1.4} \quad (31)$$

where we retain the dependence on water activity that was determined for proton and water reduction. Similarly, the current density for the reduction of HS⁻ ions is given by

$$i_{HS^-} = i_{HS^-}^0 \exp\left[\frac{-\alpha_H F(E - E_H^0)}{RT}\right] \quad (32)$$

where

$$i_{HS^-}^0 = i_{HS^-}^* a_{HS^-}^{0.3} a_{H_2O}^{1.4} \quad (33)$$

Iron dissolution

In the absence of electrochemically active species other than water and hydroxide ions, the mechanism proposed by Bockris et al.²⁶ can be used, i.e.,



This mechanism predicts that the reaction order with respect to the OH⁻ ion is 1 and the anodic transfer coefficient is equal to 1.5. Additionally, the current density for iron dissolution has been found to depend on the activity of water.³⁰ Thus, the current density for Fe dissolution is given by

$$i_{Fe} = i_{Fe}^0 \exp\left[\frac{\alpha_{Fe} F(E - E_{Fe}^0)}{RT}\right] \quad (37)$$

where i_{Fe}^0 is the exchange current density, $\alpha_{Fe} = 1.5$ and E^0 is the reversible potential of Fe dissolution. The exchange current density in acidic solutions can be expressed as

$$i_{Fe}^0 = i_{Fe}^* a_{OH}^c a_{H_2O}^c \quad (38)$$

where c is a reaction order with respect to the activity of water. According to Smart and Bockris³⁰, $c = 1.6$. The effect of the activity of water on the current density is significant only for concentrated solutions, for which the activity of water may differ significantly from one. Although the reaction order with respect to OH⁻ ions is valid for acidic solutions, it has been found that iron dissolution proceeds with little influence of pH for solutions with pH above approximately 4.^{26,28} As shown in a previous paper,²⁴ the change in the reaction order with respect to OH⁻ ions can be reproduced by assuming that the exchange current density is proportional to the surface coverage by OH⁻ ions. This assumption is consistent with the reaction mechanism (cf. eqs. 34-36). Thus, eq. (38) can be modified as

$$i_{Fe}^0 = i_{Fe}^* \theta_{OH} a_{H_2O}^c \quad (39)$$

Assuming that θ_{OH} follows the Langmuir adsorption model, eq. (39) is rewritten as

$$i_{Fe}^0 = i_{Fe}^* \frac{a_{OH}}{1 + K_{OH} a_{OH}} a_{H_2O}^c \quad (40)$$

Eq. (40) reduces to eq. (38) for low activities of OH⁻, i.e., for acidic solutions. For higher concentrations, the reaction order with respect to OH⁻ becomes zero.

The reversible potential is calculated from the Nernst equation²⁵ and depends on the activity of Fe²⁺ ions. A further relationship exists between the reversible potential and the exchange current density,³¹ i.e.,

$$\frac{RT}{\alpha_{Fe} F} \ln \frac{i_{Fe}^0}{i_{Fe}^0} = E_{Fe}^0 - E_{Fe}^0, \quad (41)$$

The exchange current density is computed from eq. (41) for any concentration of ferrous ions once it is established for any reference concentration of Fe²⁺. Thus, the current density for the iron oxidation process is a combination of eqs. (37), (40) and (41).

The presence of H₂S affects the anodic iron dissolution by the adsorption of HS⁻ ions followed by the dissolution of the adsorbed complex,^{14,32} i.e.,



Reactions (42) and (43) are followed by the hydrolysis of the adsorbed FeSH⁺_{ads} species. This mechanism is analogous to the usual, hydroxide-accelerated, mechanism of iron dissolution.¹⁴ Therefore, eq. (39) is extended by including an additional term that is proportional to the surface coverage of HS⁻ ions instead of OH⁻ ions, i.e.,

$$i_{Fe}^0 = i_{Fe}^* \theta_{OH} a_{H_2O}^c + i_{Fe}^* \theta_{SH} a_{H_2O}^c \quad (44)$$

For all partial processes, the concentration-independent part of the exchange current density (i.e., i^*) is assumed to be temperature-dependent by introducing a non-zero enthalpy of activation, i.e.,

$$i^*(T) = i^*(T_{ref}) \exp \left[-\frac{\Delta H}{R} \left(\frac{1}{T} - \frac{1}{T_{ref}} \right) \right] \quad (45)$$

IMPLEMENTATION OF THE MODEL

As described in a previous paper,¹⁴ the parameters that characterize the partial cathodic and anodic processes have been obtained from experimental data for systems that are not affected by FeCO₃ or FeS scaling. Then, the kinetic parameters that represent the effect of scale formation have been determined from a limited amount of experimental corrosion rate data. In particular, the FeCO₃ and FeS scaling parameters have been obtained using the data of Ikeda et al.⁹ and Greco et al.¹, respectively.

To compute corrosion rates using the above model, the individual processes are combined and the corrosion potential is calculated by applying the mixed-potential theory. For this purpose, the conservation-of-charge equation is solved, i.e.,

$$\sum i_{c,i} = \sum i_{a,j} \quad (46)$$

where $i_{c,i}$ and $i_{a,j}$ denote the i -th cathodic and j -th anodic process. Once the corrosion potential is obtained by solving eq. (46), the corrosion current density is also computed.

RESULTS AND DISCUSSION

Prior to applying the model to the simulation of the effect of FeCO_3 and FeS scale formation on corrosion rates, it is of interest to examine the relationship between the solubility of FeCO_3 and the calculated coverage fraction on the surface of corroding iron. Figure 1 shows the solubility of FeCO_3 in water calculated from the thermodynamic model (cf. Appendix). The calculated solubility is in good agreement with experimental data. It is noteworthy that the solubility markedly decreases with temperature at temperatures above ca. 300 K. There is a strong correlation between the decrease in solubility and the increased protectiveness of the FeCO_3 scale as the temperature rises. This is illustrated in Figure 2, which shows the calculated FeCO_3 coverage fraction as a function of temperature. The results shown in Figure 2 have been obtained from the model by using the FeCO_3 scale formation parameters (cf. eq. 12 and 8) that have been calibrated using selected corrosion rate data.⁹

Although the correlation between the solubility and coverage fraction of FeCO_3 is evident, the knowledge of solubility alone is insufficient for the prediction of the protectiveness of the scale. This is due to the fact that the precipitation of the scale-forming solid in the bulk solution (eq. 1) is not equivalent to the formation of adherent scale on the surface of corroding iron (eq. 4). From the point of view of the model, the protectiveness of the scale is primarily determined by the ratio of the reaction rate constants for the formation and dissolution of the scale on the surface of the metal. At the same time, the thermodynamic stability of the scale-forming solid depends on its solubility product, which is unrelated to the surface. These two properties may or may not coincide at given conditions, although they follow the same trends with respect to temperature.

Figure 3 shows the effect of FeCO_3 scale formation on the corrosion rate in three CO_2 -containing systems as a function of temperature. The observed maximum is a direct result of the temperature dependence of the FeCO_3 surface coverage fraction (cf. Figure 2). In the temperature range where the coverage fraction is small, the corrosion rate increases because the rates of the partial cathodic and anodic processes increase with temperature. As the coverage fraction increases with temperature, the corrosion rate reaches a maximum and then declines.

Figures 3A and 3B show the corrosion rate for iron and carbon steel, respectively, in a system where the partial pressure of CO_2 is equal to 30 bar. The values of corrosion rates are different in these two cases because of differences in the exchange current densities for the reduction of carbonic acid (eqs. 24-28) and, to a lesser extent, oxidation of iron (eqs. 34-41). However, the shape of the corrosion rate versus temperature curve and the location of the maximum are the same. This indicates that there is no substantial difference between the formation of protective FeCO_3 films on pure iron and carbon steel.

Figure 3C shows the corrosion rate of carbon steel in a system in which the partial pressure of CO_2 is 1 atm. In this case, the maximum of the corrosion rate curve is shifted toward higher temperatures. For example, the corrosion rate at 140 °C is very substantial in this case (i.e., it is greater than a half of the maximum rate) whereas the corrosion rate at $P_{\text{CO}_2} = 30$ bar and the same temperature is small (cf. Figure 3B). This behavior is explained by the dependence of the FeCO_3 coverage fraction on the partial pressure of CO_2 , which is shown in Figure 2. An increase in the partial pressure of CO_2 results in an increase in the activity of HCO_3^- ions, which, according to the model, participate in the formation of the FeCO_3 film (cf. eq. 13). This increases the coverage fraction and reduces the corrosion rate.

As shown in Figures 3A-C, the model reproduces experimental data⁹⁻¹¹ with very good accuracy. In particular, the effects of both temperature and partial pressure of CO_2 is correctly taken into account by the model.

It is of interest to examine the effect of ferrous ions in solution on the corrosion rate under conditions that may be conducive to the formation of FeCO_3 scales. Figure 4 shows the results of calculation for carbon steel at 90 °C in a solution that does not contain dissolved Fe^{2+} and in another solution that is saturated with respect to Fe^{2+} ions. At the temperature of 90 °C, the FeCO_3 coverage fraction is predicted to be fairly small. In practice, FeCO_3 coverage may or may not be obtained, depending on experimental conditions.⁵ The upper line in Figure 4 shows the corrosion rate in the absence of ferrous ions when no FeCO_3 film is formed on the surface. The middle line shows the corrosion rate when the solution is saturated with Fe^{2+} ions, but no FeCO_3 film forms. In this case, the corrosion rate is somewhat reduced, but the effect of Fe^{2+} saturation is not very strong. This effect is primarily due to an increase in pH when the solution is saturated with

respect to FeCO_3 . An increase in pH almost completely eliminates the contribution of proton reduction (eq. 16) to the cathodic process and, therefore, moderately reduces the corrosion rate. The lowest line in Figure 4 shows the corrosion rate in the presence of an FeCO_3 scale in an Fe^{2+} -saturated solution. In this case, the corrosion rates are substantially reduced. However, they remain very substantial because the FeCO_3 surface coverage at 90°C is fairly small and, subsequently, the surface scale is only moderately protective. In all cases, the model predictions are consistent with experimental data⁵ although substantial scattering of the data is observed when the FeCO_3 scale is present. It is noteworthy that the data shown in Figure 4 were not used to obtain the parameters of the model.

After examining the performance of the model for FeCO_3 scales, the model has been applied to systems where iron sulfide scales may be formed. For FeS scales, the model parameters have been calibrated using corrosion rate data for a system, in which the partial pressure of H_2S is varied continuously from 0 to 1 atm.¹ First, it is of interest to examine the FeS coverage fraction as a function of the partial pressure of H_2S . Figure 5 shows the change in the FeS coverage as the partial pressure of H_2S is varied from 10^{-7} to 1 atm while the total pressure is kept constant at 1 atm. Since the temperature is low (i.e., 30°C), the FeCO_3 coverage fraction is negligible. As shown in Figure 5, the coverage fraction becomes noticeable for the partial pressure of H_2S equal to ca. 10^{-5} atm and levels off at partial pressure exceeding 10^{-4} atm.

Figure 6 shows the effect of H_2S on the corrosion rate for the same conditions. The decline in corrosion rates at low partial pressures of H_2S parallels the increase in the FeS coverage fraction. At high H_2S partial pressures, the corrosion rate increases although the coverage fraction remains approximately the same. This is due to the additional reduction reaction of H_2S (eqs. 29-31). As the partial pressure of H_2S increases, the concentration of H_2S in the aqueous phase rises and increases the rate of H_2S reduction (eqs. 30-31). It is noteworthy that the model reproduces the combined effect of FeS scaling and H_2S reduction with very good accuracy. It should be noted that the effect of H_2S shown in Figure 6 would be somewhat altered by the presence of high concentrations of other species, such as chloride ions. However, the study of chloride effects on H_2S corrosion is beyond the scope of this work and will be considered in a future study.

The model also reproduces the pH-dependence of H_2S corrosion. This is shown in Figure 7 for a CO_2 -free system in which the partial pressure of H_2S is kept constant at 1 atm and the pH is varied by adding appropriate amounts of NaOH and H_2SO_4 . The steep decrease in corrosion rate as a function of pH, which can be observed in Figure 7, is due to two factors, i.e., the increasing effect of FeS scaling and decreasing contribution of the proton reduction reaction (eq. 16) as pH rises. The experimental corrosion rates¹⁴ are reproduced with good accuracy even though the data shown in Figure 7 were not used to calibrate the model parameters.

Finally, the model has been applied to simulate the effect of temperature on the corrosion rate in systems that contain both CO_2 and H_2S . In such systems, we can expect competition between the formation of FeCO_3 and FeS scales. While the protectiveness of FeCO_3 is a very strong function of temperature, the formation of FeS is weakly temperature-dependent. Figure 8 shows the effect of scaling for systems in which the partial pressure of CO_2 is 30 atm and the H_2S content in the vapor phase is varied from 0 to 330 ppm. Without H_2S , the corrosion rate shows a maximum that is characteristic for the effect of FeCO_3 scaling. With a low concentration of H_2S (i.e., 3.3 ppm), the maximum remains, but the peak becomes somewhat wider. With a higher concentration of H_2S (i.e., 330 ppm), the maximum essentially disappears and the corrosion rate becomes weakly dependent on temperature. This is due to the fact that FeS becomes the predominant species on the surface of the metal. The disappearance of the maximum is consistent with experimental data,¹¹ although the predicted rates are somewhat lower than the data in the low temperature range. However, this difference is acceptable in view of the differences between various sets of experimental data.^{1,11}

CONCLUSIONS

A comprehensive model has been developed for simulating the effect of FeCO_3 or/and FeS scale formation on rates of general corrosion. The model combines thermodynamic speciation calculations with electrochemical computations based on the mixed-potential theory. The electrochemical calculations recognize the effect of scaling on the various partial cathodic and anodic processes, which are responsible for corrosion. The model has been verified by comparing calculated corrosion rates with experimental data over substantial ranges of temperature, pH and partial pressures of CO_2 and H_2S . Emphasis has been put on cases that clearly demonstrate the effect of scaling on corrosion rates. Very good agreement with experimental data has been obtained. Since the model is based on a mechanistic approach to electrochemical kinetics and scale formation, coupled with detailed speciation in the aqueous phase, it can be extended to systems with more complex chemistry that go beyond $\text{CO}_2/\text{H}_2\text{S}$ systems.

REFERENCES

1. E. C. Greco, W. B. Wright, *Corrosion*, v. 18, p. 119t-124t (1962).
2. J. B. Sardisco, W. B. Wright, E. C. Greco, *Corrosion*, v. 19, p. 354t-359t (1963).
3. J. B. Sardisco, R. E. Pitts, *Corrosion*, v. 21, p. 245-253 (1965); *ibid.*, v. 21, p. 350-354 (1965).
4. F. H. Meyer, O.L. Riggs, R.L. McGlasson, J.D. Sudbury, *Corrosion*, v. 14, p. 69-75 (1958).
5. K. Videm, A. Dugstad, MP, March 1989, p. 63-67; *ibid.*, April 1989, p. 46-50.
6. K. Videm, A.M. Koren, *Corrosion*, v. 49, p. 746-754 (1993).
7. D.H. Davies, G.T. Burstein, *Corrosion*, v. 36, p. 416-422 (1980).
8. K. Videm, J. Kvarekval, *Corrosion*, v. 51, p. 260-269 (1995).
9. A. Ikeda, M. Ueda, S. Mukai, in R. H. Hausler and H. P. Godard, eds., *Advances in CO₂ Corrosion*, Vol. 1: NACE, Houston, TX, p. 39-51 (1984).
10. K. Satoh, K. Yamamoto, N. Kagawa, in R. H. Hausler and H. P. Godard, eds., *Advances in CO₂ Corrosion*, Vol. 1: NACE, Houston, TX, p. 151-156 (1984).
11. A. Ikeda, M. Ueda, S. Mukai, in P. A. Burke, A. I. Asphahani and B. S. Wright, eds., *Advances in CO₂ Corrosion*, Vol. 2: NACE, Houston, TX, p. 1-22 (1985).
12. D. W. Shoesmith, P. Taylor, M. G. Bailey, B. Ikeda, *Electrochim. Acta*, v. 23, p. 903-916 (1978).
13. D. W. Shoesmith, M. G. Bailey, B. Ikeda, *Electrochim. Acta*, v. 23, p. 1329-1339 (1978).
14. D. W. Shoesmith, P. Taylor, M. G. Bailey, D. G. Owen, *J. Electrochem. Soc.*, v. 127, p. 1007-1015 (1980).
15. D. R. Morris, L. P. Sampaleanu, D. N. Veysey, *J. Electrochem. Soc.*, v. 127, p. 1228-1235
16. E. Gulbrandsen, J.-H. Morard, J.-L. Crolet, *CORROSION/99*, paper no. 624, NACE International, Houston, TX (1999).
17. E. Dayalan, F. D. de Moraes, J. R. Shadley, S. A. Shirazi, E. F. Rybicki, *CORROSION/98*, paper no. 51, NACE International, Houston, TX (1989).
18. F.F. Lyle, *CO₂/H₂S Corrosion Under Wet Low-Flow Gas Pipeline Conditions in the Presence of Bicarbonate, Chloride and Oxygen*, Final Report PR-15-9313: PRCI, American Gas Association, Arlington, VA (1997).
19. N. Sridhar, D.S. Dunn, A. Anderko, M.M. Lencka, Final Report PR-15-9712, Pipeline Research Committee International, Arlington, VA (1998).
20. A. Anderko, P. J. Shuler, *CORROSION/98*, paper no. 64: NACE International, Houston, TX (1998).
21. A. Anderko, S.J. Sanders, R.D. Young, *Corrosion*, v. 53, p. 43-53 (1997).
22. J.F. Zemaitis, Jr., D. M. Clark, M. Rafal, N. C. Scrivner, *Handbook of aqueous electrolyte thermodynamics*: AIChE, New York, NY, 852 p. (1986).
23. M. Rafal, J. W. Berthold, N. C. Scrivner, S. L. Grise, *Models for electrolyte solutions*, in S. I. Sandler, ed., *Models for Thermodynamic and Phase Equilibria Calculations*: M. Dekker, New York, NY, p. 601-670 (1995).
24. A. Anderko, R.D. Young, *CORROSION/99*, paper no. 31, NACE International, Houston, TX (1999).
25. K. J. Vetter, *Electrochemical Kinetics*: Academic Press, New York, NY (1967).
26. J. O'M. Bockris, D. Drazic, A. R. Despic, *Electrochim. Acta*, v. 4, p. 325-361 (1961).
27. C. de Waard, D. E. Milliams, *Corrosion*, v. 31, p. 177-181 (1975).
28. S. Nesic, J. Postlethwaite, S. Olsen, *Corrosion*, v. 52, p. 280-294 (1996).
29. A. Anderko, M. M. Lencka, *Ind. Eng. Chem. Res.*, v. 37, p. 2878-2888 (1998).
30. N. G. Smart and J. O'M. Bockris, *Corrosion*, v. 48, p. 277-280 (1992).
31. J. M. West, *Electrodeposition and Corrosion Processes*: Van Nostrand, New York, NY (1964).
32. Z. A. Iofa, V. V. Batrakov, Cho-Ngok-Ba, *Electrochim. Acta*, v. 9, p. 1645 (1964).
33. H. C. Helgeson, D. H. Kirkham, G. C. Flowers, *Am. J. Sci.*, v. 281, p. 1249-1516 (1981).
34. J. C. Tanger, H. C. Helgeson, *Am. J. Sci.*, v. 288, p. 19-98 (1988).
35. L. A. Bromley, *AIChE J.*, v. 19, p. 313-320 (1973).
36. K. S. Pitzer, *J. Phys. Chem.*, v. 77, p. 268-277 (1973).
37. G. Soave, *Chem. Eng. Sci.*, v. 27, p. 1197-1203 (1972).
38. H. P. Meissner, in S.A. Newman, ed., *Thermodynamics of Aqueous Systems with Industrial Applications*: Am. Chem. Soc. Symp. Ser., v. 133, p. 495-511 (1980).

APPENDIX: THERMODYNAMIC FRAMEWORK

In a multicomponent system, the partial molal Gibbs energy of the i -th species is related to the molality (m_i) by

$$\bar{G}_i = \bar{G}_i^0 + RT \ln m_i \gamma_i \quad (\text{A-1})$$

where \bar{G}_i^0 is the standard-state partial Gibbs energy and γ_i is the activity coefficient. Thus, the thermodynamic properties of the system can be calculated if the standard-state Gibbs energies are available for all species as functions of temperature and pressure (i.e., $\bar{G}_i^0(T, P)$) and the activity coefficients are known as functions of the composition vector \mathbf{m} and temperature (i.e., $\gamma_i(\mathbf{m}, T)$). From basic thermodynamics, the standard-state Gibbs energy of formation $\bar{G}_i^0(T, P)$ can be calculated as a function of temperature and pressure if the following data are available:

- (1) Gibbs energy of formation at a reference temperature and pressure (usually, $T_r = 298.15$ K and $P_r = 1$ bar);
- (2) Enthalpy of formation at T_r and P_r ;
- (3) Entropy at T_r and P_r ;
- (4) Heat capacity as a function of temperature and pressure and
- (5) Volume as a function of temperature and pressure

The key to representing the standard-state properties over substantial temperature and pressure ranges is the accurate knowledge of the heat capacity and volume as functions of temperature and pressure. Then, the Gibbs energy and remaining functions can be obtained by integration using standard thermodynamic formulas. To express the temperature and pressure dependence of standard-state thermodynamic properties of aqueous species, the Helgeson-Kirkham-Flowers-Tanger (HKFT)^{33,34} equation of state is used. The HKFT equation is based on the solvation theory and expresses the standard-state thermodynamic functions as sums of structural and solvation contributions, the latter being dependent on the properties of the solvent (i.e., water). In its revised form³⁴, the HKFT equation is capable of reproducing the standard-state properties up to 1000 °C and 5 kbar. The expressions for the standard-state thermodynamic functions are given in the original papers³⁴ and are summarized in a review.²³

The activity coefficient model used for representing the solution nonideality is an extended form of an expression developed by Bromley.³⁵ The extended Bromley equation is a combination of the Debye-Hückel term for long-range electrostatic interactions and a semi-empirical expression for short-range interactions between cations and anions. In a multicomponent system, the activity coefficient of an ion i is given by

$$\log \gamma_i = \frac{-Az_i^2 I^{1/2}}{1 + I^{1/2}} + \sum_j^{NO} \left[\frac{|z_i| + |z_j|}{2} \right]^2 \left[\frac{(0.06 + 0.6B_{ij})|z_i z_j|}{\left(1 + \frac{1.5}{|z_i z_j|} I\right)^2} + B_{ij} + C_{ij} I + D_{ij} I^2 \right] m_j \quad (\text{A-2})$$

where A is the Debye-Hückel coefficient which depends on temperature and solvent properties, z_i is the number of charges on ion i , I is the ionic strength (i.e., $I = 0.5 \sum z_i^2 m_i$), NO is the number of ions with charges opposite to that of ion i , and B_{ij} , C_{ij} and D_{ij} are empirical, temperature-dependent cation-anion interaction parameters. Bromley's original formulation³⁵ contains only one interaction parameter, B_{ij} , which is sufficient for systems with moderate ionic strength. For concentrated systems, the two additional coefficients C_{ij} and D_{ij} usually become necessary. The three-parameter form of the Bromley model is capable of reproducing activity coefficients in solutions with very high ionic strengths, which cover the composition range of the refrigeration working fluids. The temperature dependence of the B_{ij} , C_{ij} and D_{ij} parameters is usually expressed using a simple quadratic function.

The Bromley model is restricted to interactions between cations and anions. For ion-molecule and molecule-molecule interactions, the well-known model of Pitzer³⁶ is used. To calculate the fugacities of components in the gas phase, the Redlich-Kwong-Soave³⁷ equation of state is used.

In the absence of sufficient experimental data, reasonable predictions can be made using a method due to Meissner,³⁸ which makes it possible to extrapolate the activity coefficients to higher ionic strengths based on only a single, experimental or predicted, data point.

LIST OF SYMBOLS

a_x	activity of species X
E	potential
E^0	equilibrium potential
F	Faraday constant
G_i	partial molal Gibbs energy
i	current density
i^0	exchange current density
i^*	factor in the equation that relates the exchange current density to activities of species
i^p	current density modified by the presence of scales
j_i	rate constant for the formation of i-th solid species
k_m	mass transfer coefficient
K_{MeX}	solubility product for the salt MeX
K_X	adsorption equilibrium constant for species X
l_i	rate constant for the dissolution of i-th solid species
q_i	composite parameter defined by eq. (11)
R	gas constant
t	time
T	temperature

Greek letters

α	electrochemical transfer coefficient
γ	activity coefficient
ΔH	enthalpy of activation
Δq_i	parameter determining the temperature dependence of q_i
θ_i	fraction of surface occupied by i-th species
σ_x	surface concentration of species X

Superscripts

a	activation-controlled
lim	limiting

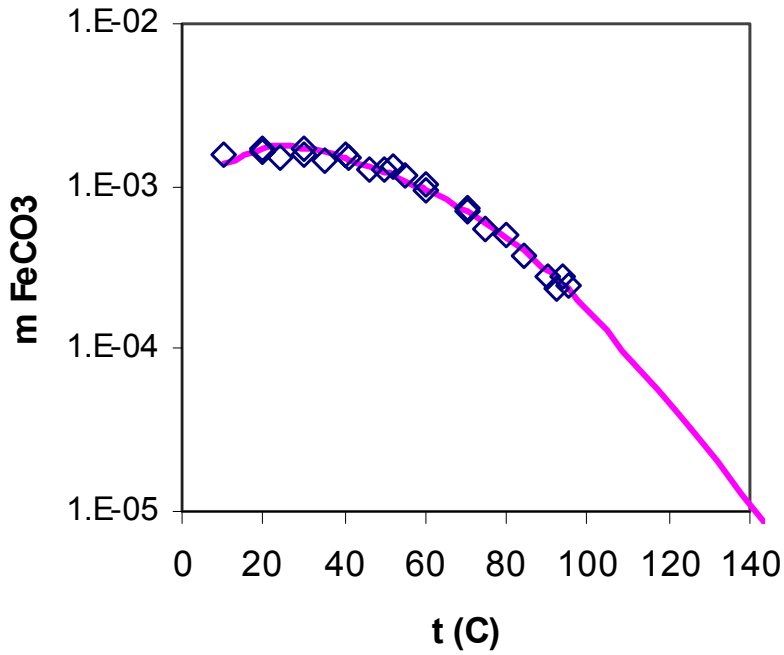


Figure 1. Solubility of iron carbonate in water as a function of temperature. The line has been obtained from the thermodynamic model and the symbols denote experimental data.

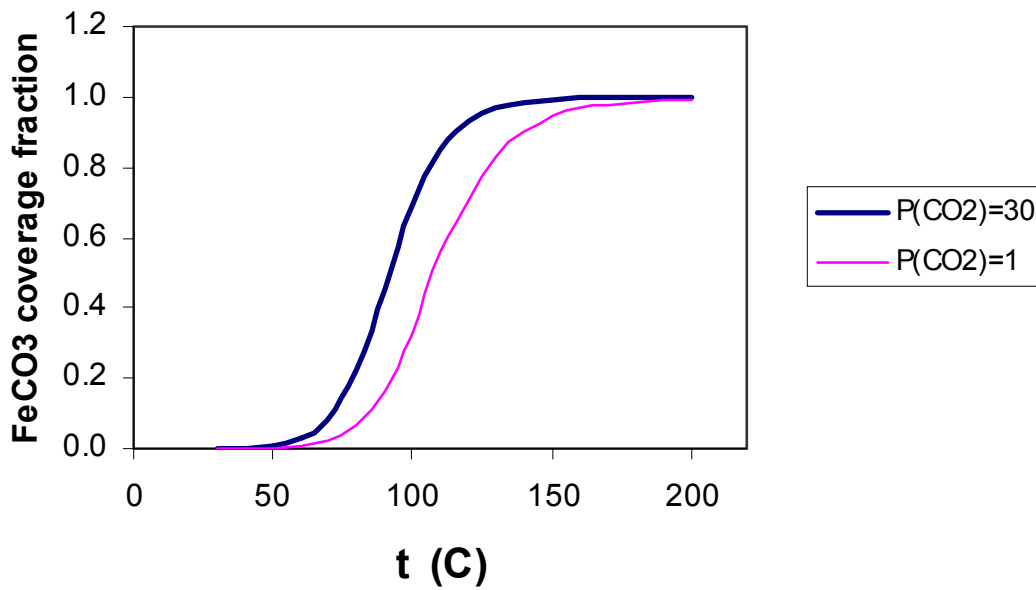
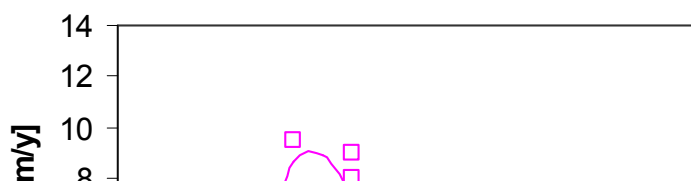
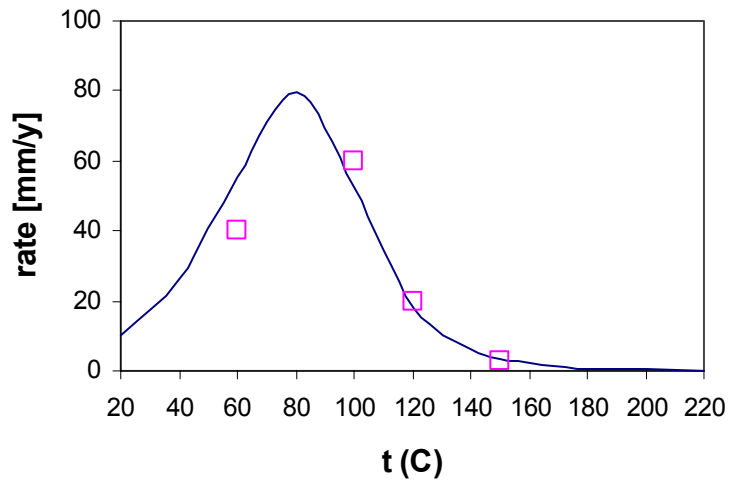


Figure 2. Calculated FeCO₃ surface coverage fraction as a function of temperature for iron in H₂O + CO₂ systems with the partial pressure of CO₂ equal to 1 or 30 atm.



A

B



C

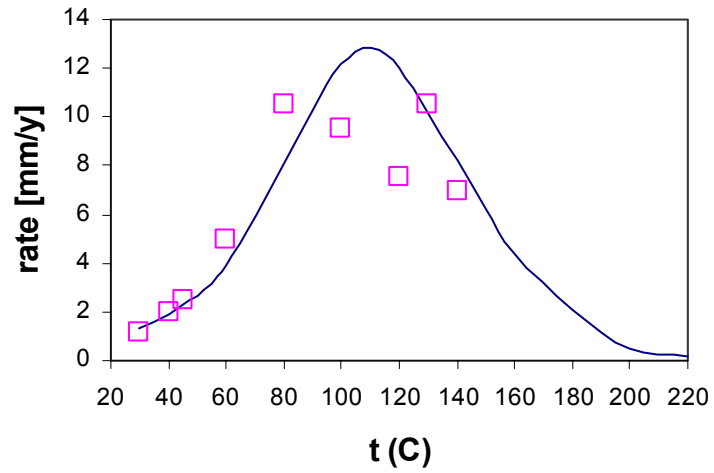


Figure 3. Effect of FeCO_3 scale formation on the corrosion rate as a function of temperature for iron in 0.9 m NaCl solution (case A), carbon steel in synthetic seawater (case B) and carbon steel in 0.017 m NaCl solution (case C). The lines have been calculated from the model and the symbols denote the data of Ikeda et al.⁹ (cases A and B) and Satoh et al.¹⁰ (case C).

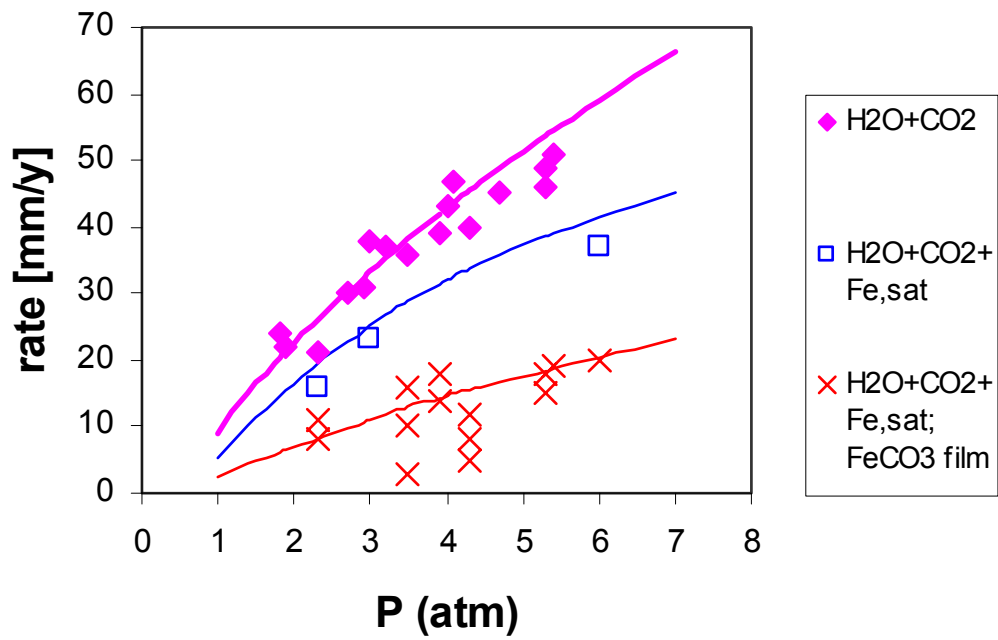


Figure 4. Corrosion rate of St. 52 carbon steel at 90 °C under various conditions, i.e., (A) in a solution that does not contain ferrous ions and in the absence of a FeCO_3 film; (B) in a solution saturated with FeCO_3 and in the absence of an FeCO_3 film and (C) in a solution saturated with FeCO_3 and in the presence of an FeCO_3 film. The lines have been obtained from the model and the symbols denote the experimental data of Videm and Dugstad.⁵

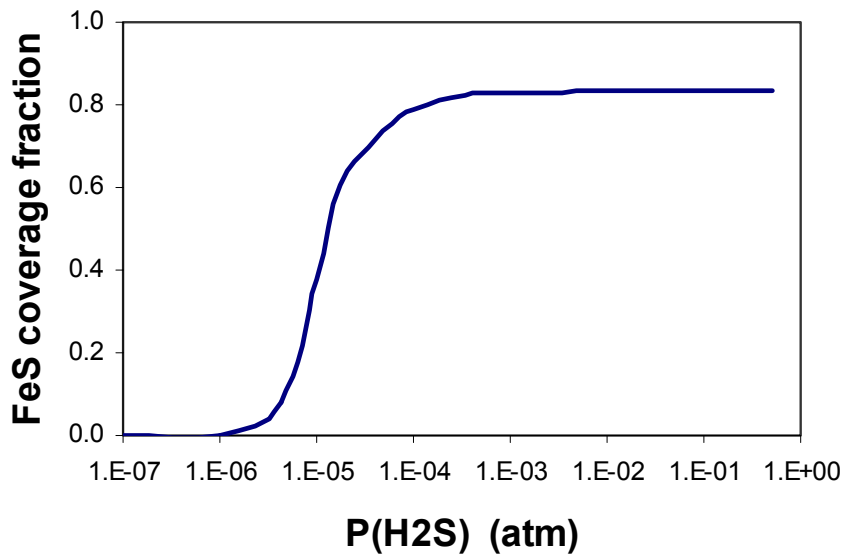


Figure 5. Calculated FeS surface coverage fraction as a function of H_2S partial pressure for iron in an aqueous solution of CO_2 and H_2S with the total pressure of 1 atm at 30 °C.

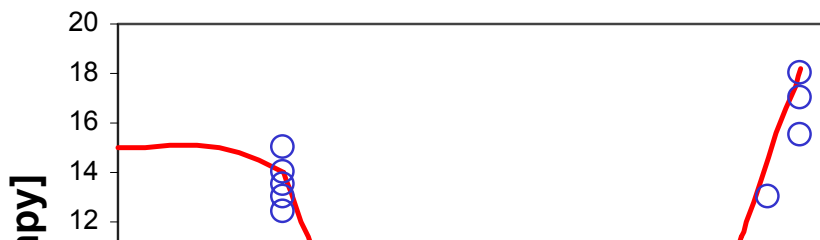


Figure 6. Corrosion rate of iron as a function of H₂S partial pressure for iron in an aqueous solution of CO₂ and H₂S with the total pressure of 1 atm at 30 °C. The line has been obtained from the model and the symbols denote the data of Greco and Wright.¹

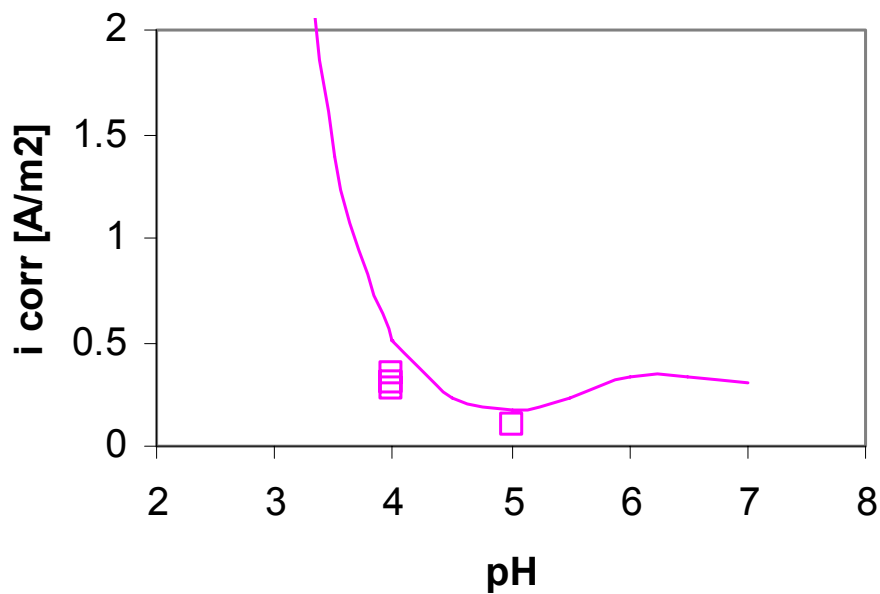


Figure 7. Corrosion rate of iron in an H₂S saturated solution at 21 °C and 1 atm as a function of pH. The solution pH was varied by adding appropriate amounts of H₂SO₄ and NaOH. The lines have been obtained from the model and the symbols denote the data of Shoemsmith et al.¹⁴



Figure 8. Effect of H₂S concentration on the corrosion rate of iron as a function of temperature in a 0.9 m NaCl solution with a partial pressure of CO₂ equal to 30 bar. The lines have been calculated using the model and the symbols denote the data of Ikeda et al.¹¹